Fusion Engineering and Design 112 (2016) 388–392

Contents lists available at ScienceDirect

Fusion Engineering and Design

journal homepage: www.elsevier.com/locate/fusengdes

Simulation of microexplosion hydrodynamics in heavy ion fusion reactor chamber with wetted first wall

S.A. Medin[a,c,*], M.M. Basko[b,c], Yu N. Orlov[b,c], V.M. Suslin[b]

[a] Joint Institute for High Temperatures, RAS, Izhorskaya 13, Bd 2, 125412 Moscow, Russian Federation
[b] Keldysh Institute for Applied Mathematics, RAS, Miusskaya 4, 125047 Moscow, Russian Federation
[c] Moscow Institute of Physics and Technology, Kerchenskaya 1A, Bd 1, 117303 Moscow, Russian Federation

HIGHLIGHTS

- Thermonuclear explosion of a HIF target is simulated with the 1D DEIRA code.
- Fireball expansion in the reactor chamber is simulated with the 1D RAMPHY code.
- The two simulations are combined to find the response of the wetted chamber wall.
- The liquid wall film is modestly shocked by X-rays and evaporated mainly by target debris.

ARTICLE INFO

Article history:
Received 4 February 2016
Received in revised form 26 June 2016
Accepted 27 June 2016
Available online 18 July 2016

Keywords:
Heavy ion fusion
Cylindrical target
Thin-liquid first wall
Fireball expansion
Reactor chamber response

ABSTRACT

Thermonuclear fusion flare, fireball expansion, and evaporation of the liquid-film chamber wall are simulated by combining two one-dimensional (1D) codes DEIRA and RAMPHY. The considered process is divided into two phases: the DEIRA code is used to simulate the fast ignition and burn of a cylindrical target with DT fuel and a lead tamper, while the RAMPHY code is applied to describe the subsequent quasi-spherical expansion of the fireball. By the end of the first phase, the neutron and X-ray output from the target as well as the debris motion are determined. The fast ions are practically fully absorbed by the lead tamper of the fusion target. At the second stage, which starts with the arrival of the main shock at the target surface, the fireball expansion and the behavior of the wall liquid film are considered. The fireball front propagates with a velocity close to the self-similar value. The liquid film is first evaporated by the X-ray pulse, and then by the heat flux generated when the fireball collides with the primary vapor layer. Mechanical loading on the liquid film remains within the 100-MPa range.

1. Introduction

The hydrodynamics in a heavy ion fusion reactor chamber can be divided into two principal stages, (a) implosion and burn of the DT fuel in the target, and (b) particle and radiation deposition on the first wall and debris propagation through the chamber cavity atmosphere. Fast ignition with heavy ion beams is now being considered as a promising alternative option for target design [1,2]. The fast ignition concept is based on successive compression and ignition of deuterium-tritium fuel by two separate heavy ion pulses. The DT fuel is placed in a high-density case, which facilitates fuel compression and confinement. A simple target design has a cylindrical configuration, initially consisting of a DT cylinder surrounded by a heavy metal shell. The target is irradiated by ion beams along the axis. The first beam has a hollow shape and drives the shell implosion resulting in fuel compression. Next, the compressed fuel is ignited by a short and tightly focused second ion beam, which initiates a burn wave propagating through the fuel. The earlier radiation hydrodynamics simulations [3–5] have lead to the following parameters for efficient heavy ion cylindrical target drive: 100 GeV for the energy of ions, 4 MJ for the deposited compression beam energy, 0.4 MJ for the ignition threshold beam energy, and 0.5 g/cm^2 for the $(\rho R)_{DT}$ parameter. These criteria may be made less severe in the new concept of an X-target with a quasi-spherical fuel compression [2].

The fusion reactions in such a target produce particle and radiation fluxes impacting on the first wall and the atmosphere of the reactor chamber. In the cylindrical target the fuel burn fraction amounts to 0.4 with relative energy partition of 0.78 in neutrons,

* Corresponding author at: Joint Institute for High Temperatures, RAS, Izhorskaya 13, Bd 2, 125412 Moscow, Russian Federation.
E-mail address: medin@ihed.ras.ru (S.A. Medin).

http://dx.doi.org/10.1016/j.fusengdes.2016.06.052
0920-3796/

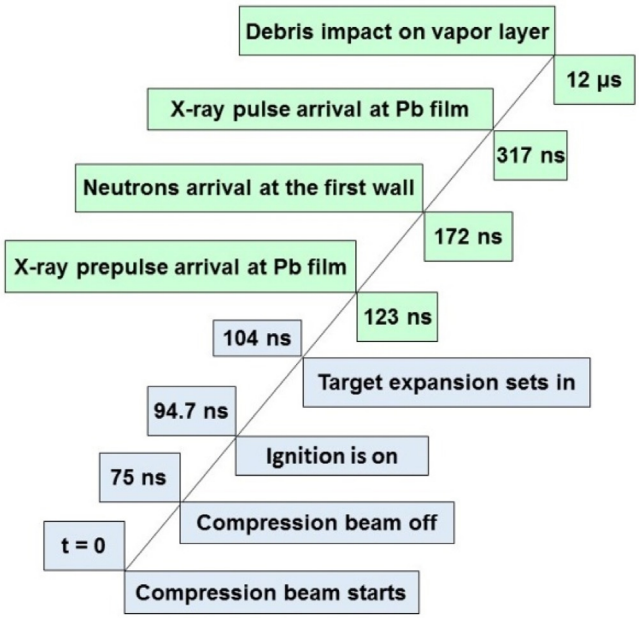

Fig. 1. The sequence of events in computational history.

0.02 in X-rays and 0.20 in ion debris. Most of the alpha-particles are absorbed in the target material. Under these conditions the protection of the first wall is provided by a thin liquid film of metal coolant [6,7].

The X-rays deposition in the liquid film produces decaying shocks of moderate intensity (~100 MPa) and results in partial evaporation of the liquid [2].

In this paper, the hydrodynamics of the cylindrical target compression and burn, followed by the fireball expansion and the liquid film evaporation are simulated in a combined computational scenario. The first part of the paper deals with the results from the 1D-3T radiation hydrodynamics code DEIRA [8], employed for description of the target microexplosion. The data on the dynamics of the lead shell implosion under the compression beam and the initial stage of the target expansion after the DT fuel flare are discussed. In the second part, the results for spherical expansion of the fireball, simulated with the 1D-2T radiation hydrodynamics code RAMPHY [9], are presented. In this latter code, the wide-range equation of state taking into account the liquid metal vaporization and ionization [10] and X-ray volumetric energy deposition are used. The computations have been performed for spherical volume of a reactor chamber of 5 m radius protected by a thin lead film. The shock propagates through the atmosphere with an approximately constant velocity (≈400 km/s) and impacts on a layer of evaporated lead film close to the first wall. The sequence of events for the microexplosion is presented in Fig. 1. The time of ignition is taken at the moment of maximum fuel compression, 94.7 ns. The shock initiated in the lead shell by the fuel flare reflects from the target free surface as a release wave at 104 ns, which is accompanied by emission of a short intense X-ray prepulse. The main X-ray radiation pulse starts at 300 ns.

2. Simulation of target compression and fuel flare

2.1. Computational model

Computation of the target heating by ion beams and DT fuel burn is performed using the 1D-3T Lagrangian code DEIRA [8]. The physical model of the DEIRA code includes

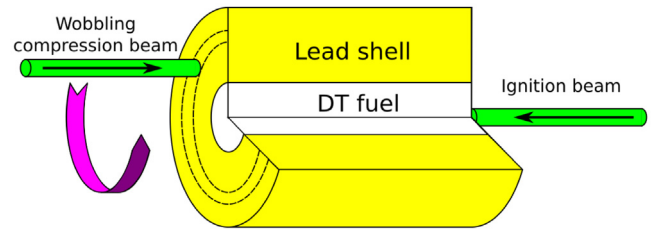

Fig. 2. The cylindrical target for fast ignition heavy ion fusion.

- electron and ion thermal conduction and temperature relaxation, ion viscosity,
- electron and ion heating rates by all thermonuclear products,
- radiation diffusion and relaxation between electron and radiation temperatures,
- diffusion and relaxation of energy of fast charged fusion products
- mean Rosseland and Planckian opacities,
- two-temperature equation of state,
- thermonuclear burn rates (DT, DD, DHe^3) without in-flight reactions,
- external energy deposition by solving the stopping equation for fast heavy ions.

The code DEIRA has been validated against analytical solutions of the following problems: ion-electron temperature relaxation behind the strong shock, heat and radiation waves propagation and energy density diffusion of fast fusion products.

2.2. Cylindrical target input data specification

The cylindrical target design is chosen according to previous simulation data [3,4]. The DT fuel cylinder with a radius of 1.12 mm is surrounded by a lead shell with a radius of 4 mm (Fig. 2). For the target length of 6.4 mm, the masses of fuel and lead are equal to 5.7 mg and 3.4 g, respectively. At the compression stage, the target is irradiated by a hollow (annular) beam of 125 GeV ^{209}Bi ions. The hollow irradiation pattern is supposed to be arranged by means of rotation of a filled beam focused in the spot of 1.25 mm diameter. The spot moves at the target end surface along a circle of 3.75 mm diameter with a frequency of 1 GHz. The high frequency of the focal spot rotation assures azimuthally uniform ion energy deposition in the lead shell. The axial uniformity of energy deposition is assumed under the condition that the target length is less than the ion range. The ion-range for 125 GeV ^{209}Bi is of the order of 10 mm. This lets the Bragg peak outside the working target length of 6.4 mm. In our 1D computations the deposited compression beam energy amounts to 4.37 MJ.

The profiled ion pulse consists of 20 ns prepulse and the main pulse at $44\,\text{ns} \le t \le 75\,\text{ns}$ with the peak plateau of 336 TW at $44\,\text{ns} \le t \le 75\,\text{ns}$. The optimized beam profiling results in very low entropy increase in the process of fuel compression.

The ion beam heating is implemented as an energy source for the target electrons. The specific energy deposition is proportional to the ion beam intensity and the stopping power of the shell material. In the 1D approximation, the stopping power is averaged along the ion beam direction. The radial profile of the irradiation intensity in the focal spot is taken as an inverted parabola.

In our 1D approximation, the irradiation by the ignition pulse is modeled as a uniform volumetric deposition of the energy 3.93 MJ over the entire compressed DT cylinder, turned on after the threshold value of the DT density-radius product $\rho R = 0.5$ has been reached. This value of the deposited energy is substantially higher than the initiation energy of 0.4 MJ for 2D modeling in references

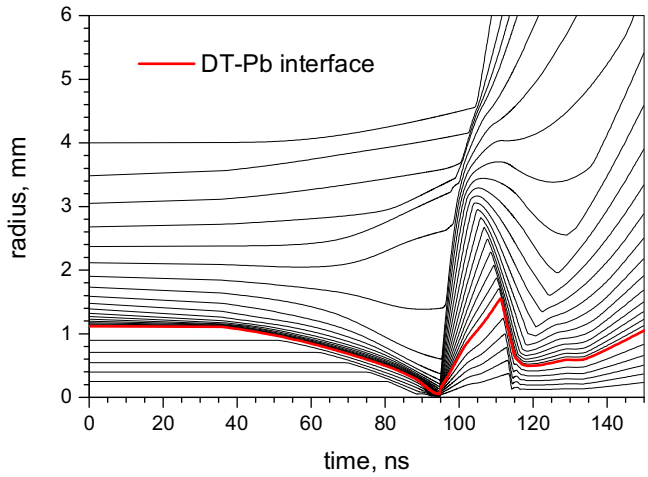

Fig. 3. The time-space diagram for the cylindrical target. At $t = 0$ the boundary between the DT fuel and the Pb shell is located at $r = 1.22$ mm.

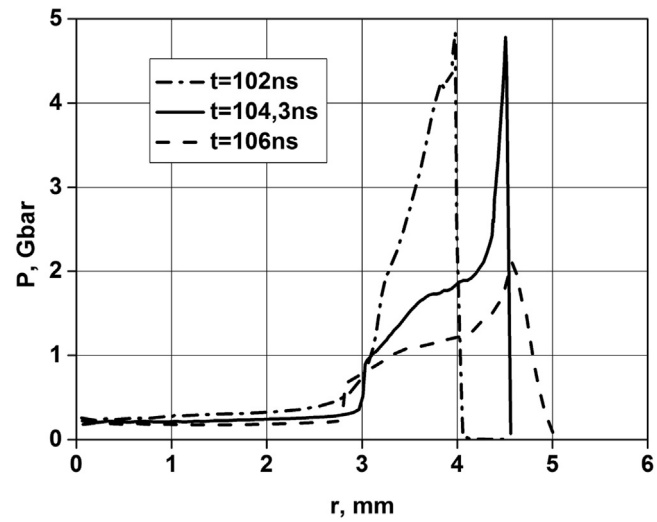

Fig. 4. Radial profiles of pressure at the shock arrival at the free surface of the target.

[3–5]. This is explained by different burning modes in these two cases. In the 2D approximation, a detonation wave was initiated which propagated along the cylinder and ignited the cold fuel, while in the 1D approximation we are forced to resort to a simpler volume ignition mode. Within such a procedure, we lose all the details of the 2D burn wave propagation along the fuel cylinder and strongly (by about a factor of 10) overestimate the deposited energy, required for ignition and efficient burn in the realistic 2D case [3–5]. However, these details are not important for the overall target output balance.

2.3. Dynamics of the target ignition and characterization of explosion products

Rapid compression of the DT fuel begins after the power rises to its maximum in the main part of the ion pulse at $t \approx 40$ ns. In Fig. 3 the time-space diagram for the material flow is drawn. The fuel compression, as well as outward displacement of the cold lead layer, occurs due to the expansion of the dense lead plasma. After the thermonuclear flare energy has been released at 94.7 ns, a strong shock is generated in the plasma. The shock travels through the lead shell, reflects and refracts at the cold external layer and, finally, appears at the free surface of the target.

The shock arrival at the target surface is illustrated in Fig. 4. The arrival time is equal to 104.3 ns. The shock is reflected from the free surface as a rarefaction wave. In the rarefaction wave, a short prepulse of X-ray emission is generated. The peak power of the prepulse amounts to 240 TW, with the surface radiation temperature of 187 eV, whereas in the incident shock the peak radiation temperature reaches 1.08 keV. The main pulse of X-rays appears significantly later, near 300 ns (see Fig. 5), when the plasma fireball becomes more transparent for the X-ray radiation. It has rather long duration with FWHM of 360 ns and a relatively low amplitude of 27.7 TW. The total emitted X-ray energy amounts to 15.8 MJ. Such relatively mild temporal characteristics of the main X-ray pulse, explained by a large mass of the lead tamper, result in a relatively soft impact on the first chamber wall.

The fuel burn produces a pulse of 14-MeV neutrons with a FWHM of 100 ps. The temporal profile of the neutron flux is shown in Fig. 6. The total energy of the neutron pulse is 587 MJ, of which 9.1 MJ is deposited in the target.

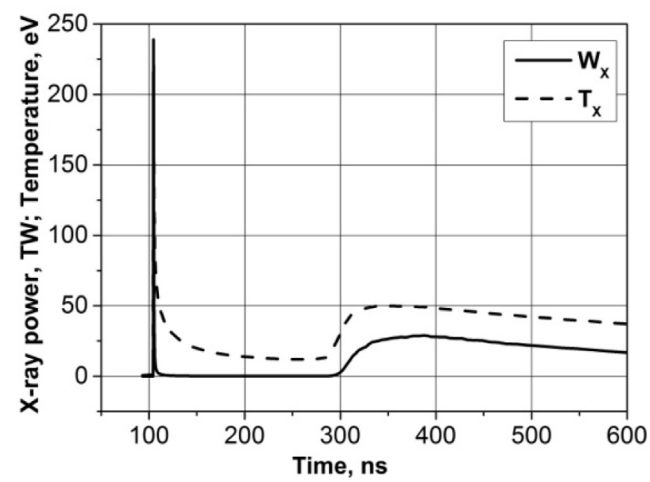

Fig. 5. Temporal profiles of the radiation temperature and of the total power of the X-rays emitted by the external surface of the expanding target.

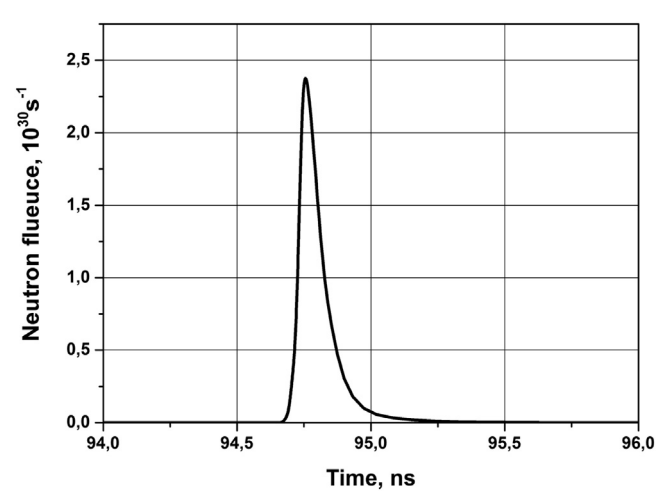

Fig. 6. The temporal profile of the flux of 14-MeV neutrons generated in the DT fuel flare.

3. Fireball expansion and liqiud film evaporation

3.1. Computational model and the input data

The computations of the fireball expansion are initiated at the moment of the shock appearance at the target surface. According to the sequence of events, shown in Fig. 1, the shock propagation through the spherical reactor chamber of 5 m radius and the impact of the X-ray radiation on a liquid protection layer of 2 mm thickness are to be simulated. This is carried out with the code RAMPHY, which has been specially developed for simulations of the reactor chamber flow. RAMPHY is a 1D-2T Lagrangian radiation-hydrodynamics code [9], allowing for

- plasma thermal conduction and viscosity,
- radiation diffusion and relaxation between plasma and radiation temperatures
- mean Rosseland and Planckian opacities,
- neutron diffusion and heating (Monte Carlo N–Particle Transport Code System [11]),
- condensed matter strength and spallation,
- wide-range equation of state, phase transitions and ionization,
- external energy sources: X-ray and fast ions volumetric energy deposition.

The simulation of the fireball expansion starts at 104.3 ns, when the shock has arrived at the cylindrical target surface. The distributions of the principal physical variables in the expanding fireball, obtained as described in Section 2, are used as an input to the RAMPHY code.

The initial parameters of the reactor chamber atmosphere and the liquid film are fixed according the equilibrium conditions at the temperature of 823 K. The initial gas chamber density equals 3.5×10^{-10} g/cm^3. The vapor mass in the chamber is 0.18 g. The computations are performed in the spherical geometry in order to match the 1D flow to the chamber geometry. The reactor chamber in the FIHIF concept is characterized by the shape irregularity [7]. But the upper section where the target is shot has cylindrical geometry with equal diameter and height. For spherical fireball expansion the substantial part of the first wall there has near-identical loading. For qualitative assessment of the first wall response we take the spherical symmetry of the chamber.

The cylindrical-spherical geometry transition at $t = 104.3$ ns was accomplished by remapping the cylindrical Lagrangian cells of 6.4 mm length from DEIRA code into spherical ones under condition of equal masses and densities of the transformable cells. The grid values of velocity, pressure, temperature and other parameters were translated to the spherical cells from the cylindrical cells. For the radiation power emitted from the sphere surface during the X-ray prepulse the DEIRA computed profile was used (see Fig. 5). Such a transformation allows adequate reproduction of the later phase of the fireball expansion, when the influence of the initial fireball structure becomes negligible, i.e. under the condition$r \gg r\{t = 104.3ns\}$.

3.2. Hydrodynamics of the fireball expansion and liqiud film evaporation

The initial impact of the target microexplosion on the reactor chamber is produced by the X-ray prepulse. Absorption of the X-ray prepulse results in generation of a shock inside the liquid film of the first wall. Earlier, in Ref. [12], the pressure wave traveling across the film has been computed. In Fig. 7 the pressure distributions are plotted at various times. The maximum pulse pressure amounts to 2×10^8 Pa. The energy deposition by neutrons raises the pressure profile at $t = 175$ ns almost uniformly across the film due to their large range.

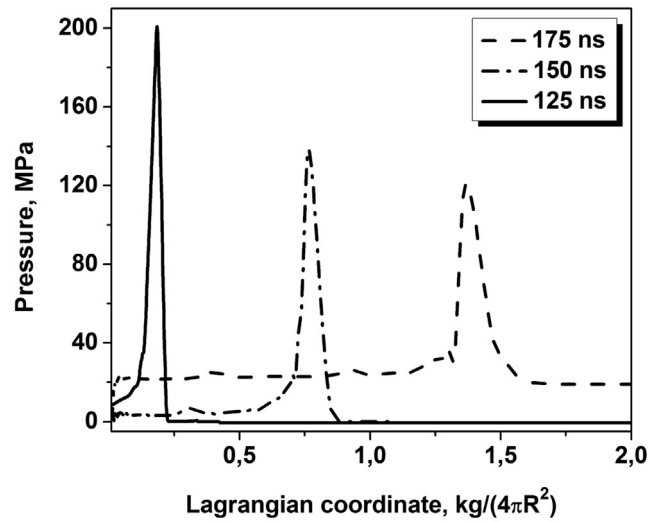

Fig. 7. Pressure wave in the liquid film produced by the X-ray prepulse.

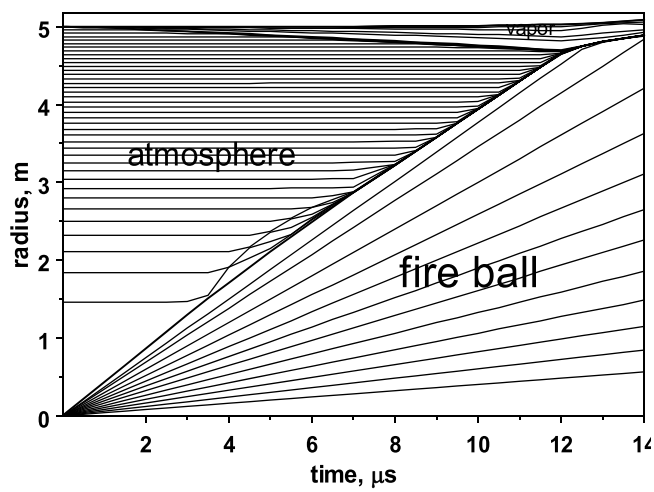

Fig. 8. The time-space diagram of the spherical fireball expansion, atmosphere contraction and liquid film vaporization.

The energy of the X-ray prepulse is too low, about 0.2 MJ, to cause significant liquid evaporation. This, however, occurs during the main X-ray pulse of 15 MJ, which evaporates some 1.5 kg of liquid film. The intensity of the main X-ray pulse is relatively low (see Fig. 5). So the shock strength is 3 times lower than that from the X-ray prepulse.

The dynamics of the target fireball expansion, the contraction of its atmosphere and the ablation of the liquid film are illustrated in Fig. 8. There are two waves in the reactor chamber propagating in opposite directions. The first wave is produced by the fireball expansion and propagates with an approximately constant velocity of 380 km/s. The second wave is caused by the expansion of vapor generated at the wetted wall and moves with the 39 km/s velocity. The two waves collide in about 12 μs after the flare. The radial profiles of pressure in the fireball and in the evaporated layer are presented Fig. 9. Four pairs of curves are plotted for time moments $t = 3$; 7; 10 and 12 μs. For convenience the upper parts of the vapor curves are cut.

The maximum peak of the vapor pressure occurs at the time t = 12 μs of shock collision and equals 5 MPa; after the shock collision it drops off. Before the collision, some 1.5 kg of liquid lead is

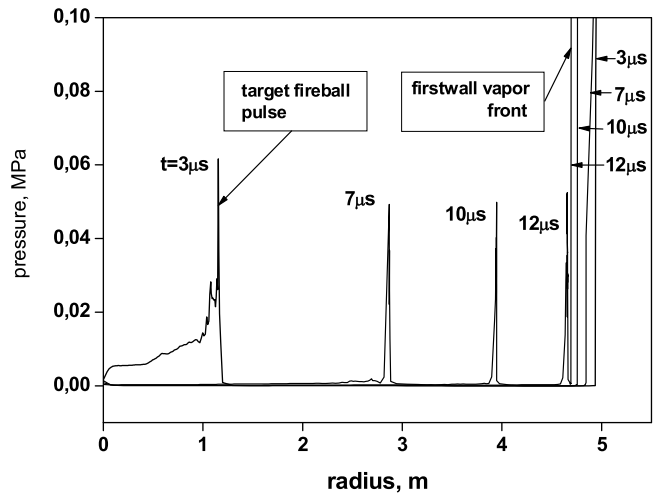

Fig. 9. Pressure profiles in the course of expansion of the fireball and of the evaporated wall film.

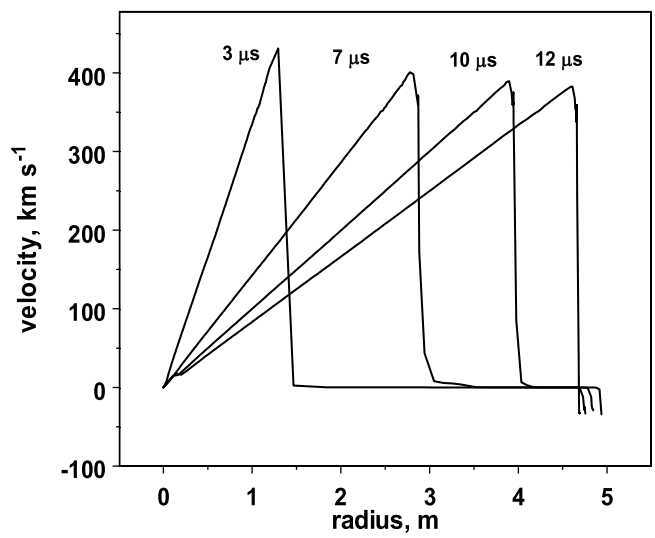

Fig. 10. The velocity distribution in the reactor chamber at various moments.

evaporated under the X-ray irradiation by the fireball. Collision of the two shocks leads to a significant rise of temperature and causes additional vaporization of the liquid film, eventually amounting to 15 kg.

The radial distributions of the matter velocity are plotted in Fig. 10. Practically linear velocity profile is formed within the fireball. This profile is close to the Sedov's self-similar solution for spherical expansion of gas into vacuum [13]. This could be expected because of the high ratio between the fireball and the atmosphere masses. At the fireball surface, a thin shocked layer of the atmosphere is formed. The evaporated lead moves away from the chamber wall, which is manifested by the negative branches of the velocity curves.

4. Conclusions

Hydrodynamics of fast ignition and burn of a heavy ion fusion target, followed by the fireball expansion and the liquid film evaporation in the reactor chamber with the wetted first wall, have been studied numerically. In view of the large difference in dimensions and time scales between the target and the reactor chamber, two complementary 1D codes DEIRA and RAMPHY in, respectively, cylindrical and spherical geometries have been used. Simulation of the target compression and burn stage has demonstrated that an appropriately shaped ion energy deposition in the lead tamper ensures practically isentropic compression of the DT fuel. When the density-radius of the fuel cylinder reaches 0.51 g/cm^2, the ignition and burn are initiated by additional energy deposition. The output spectrum from the target is determined by a neutron pulse and X-ray radiation, while most alpha particles are absorbed by the thick lead tamper. The neutron flux produces a modest quasi-volumetric loading of the wall liquid film, while the X-ray radiation causes appreciable evaporation and a moderate shock wave in the liquid film.

The target fireball expansion in the reactor chamber proceeds with an almost constant velocity. At the outer rim of the fireball, a thin shocked layer of the atmosphere builds up. The fireball expansion ends by a hypervelocity impact on evaporated layer of the first liquid wall. As a result, a considerable mass of the liquid film is vaporized. The incident shock decays rapidly in the vapor layer.

The presented data indicate that the initial response of the liquid first wall to the DT target microexplosion occurs under tolerable conditions. The thin liquid film is able to protect properly the blanket material from the X-ray radiation and the debris flow generated by the explosion of the thermonuclear target. For the final decision on the conceptual design of the first wall, a multi-dimensional modeling of radiation-hydrodynamics and mechanics of solids is to be performed. The effect of other subsequent events in the reactor chamber like, for instance, the liquid film splashing, vapor condensation, droplet sedimentation is to be evaluated.

Acknowledgments

This work is supported by the Russian Foundation of Basic Research under contract 15-08-02575 A. We are very grateful to the anonymous reviewer for comments that improved the quality of this manuscript.

References

[1] B. Yu Sharkov, et al., Nucl. Instrum. Methods A 577 (2007) 14.
[2] E. Henestroza, B.G. Logan, Phys. Plasmas 19 (2012) 072706.
[3] M.M. Basko, et al., Laser Part. Beams 20 (2002) 411.
[4] V.V. Vatulin, O.A. Vinokurov, Laser Part. Beams 20 (2002) 415.
[5] R. Ramis, J. Meyer-ter-Vehn, Laser Part. Beams 32 (2014) 41.
[6] L.M. Waganer, Fusion Eng. Des. 25 (1994) 125.
[7] S.A. Medin, et al., Laser Part. Beams 20 (2002) 419.
[8] M.M. Basko, DEIRA 1D-3T Hydrodynamic Code for Simulating ICF Targets Driven by Fast Ion Beams, ITEP, Moscow, 2001.
[9] M.M. Basko, *et al.* Keldysh Inst. Appl. Mathem., Preprint 18, March 2010 (in Russian).
[10] A.B. Medvedev, in: V.E. Fortov, L.V. Al'tshuler, R.F. Trunin, A.I. Funtikov (Eds.), High-Pressure Shock Compression of Solids VII, Springer-Verlag, 2004, p. 403.
[11] Monte Carlo N–Particle Transport Code System, Los Alamos National Laboratory, 2008, October.
[12] S.A. Medin, et al. 33rd EPS Conf. on Plasma Phys. Rome, 19–23 June 2006, ECA Vol. 30I, O-2.012 (2006).
[13] L.I. Sedov, Similarity and Dimensional Methods in Mechanics, Academic Press, New York, 1959.